Supporting Information

Nickel single atom mediated phosphate functionalization of moss derived biochar effectively enhances electrochemical uranium extraction from seawater

Huachuan Feng[1#], Huanhuan Dong[1#], Pan He[2#], Junhui He[3], Enmin Hu[1], Zishu Qian[1], Jin Li[1], Jiejie Li[1], Wenkun Zhu[,1], Tao Chen*[,1]*

1. State Key Laboratory of Environment-friendly Energy Materials, National Co-innovation Center for Nuclear Waste Disposal and Environmental Safety, Sichuan Co-Innovation Center for New Energetic Materials, Nuclear Waste and Environmental Safety Key Laboratory of Defense, School of Life Science and Engineering, Southwest University of Science and Technology, Mianyang, Sichuan 621010, P. R. China.

2. College of Chemistry, Key Laboratory of Radiation Physics & Technology, Ministry of Education, Sichuan University, Chendu, Sichuan 610064, P. R. China.

3. Department of Materials Engineering, Sichuan College of Architectural Technology, Sichuan 618000, P. R. China

 # These authors contributed equally to this work.

∗Corresponding authors.

E-mail addresses: zhuwenkun@swust.edu.cn (W. Zhu), chent@swust.edu.cn (T. Chen).

1. Experimental section

1.1 Material and Chemicals

The *R. japonicum* L was collected from Zhangjiajie. Dicyandiamide ($C_2H_4N_4$), nickel (II) chloride hexahydrate ($NiCl_2 \cdot 6H_2O$), 70% phytic acid solution, and ethanol were purchased from Aladdin Biochemical Technology Co., Ltd. (Shanghai, China). All experiments were conducted using ultrapure water (UPW) with a resistivity of 18.25 $m\Omega \cdot cm^{-1}$, and no further purification was performed on any other reagents before use.

1.2 Activity evaluation of catalysts

The prepared sample is utilized as a catalyst for electrocatalytic uranium extraction. Unless otherwise specified, all experiments are conducted in a three-electrode electrochemical workstation with Ag/AgCl as the reference electrode, using a material concentration of 0.1 mg·ml-1. and a voltage of -1.8 V.

After the electrocatalysis, the quantities of UO_2^{2+} were measured by UV-Vis (wavelength of 651.8 nm).

A formula following as the determining of the ratio of U(VI) removal during photocatalysis:

$$\text{removal ratio} = \text{removal ratio} = \frac{C_0 - C_t}{C_0} \times 100\% \quad (1)$$

In this formula, C_0 takes for the initial $C_{U(VI)}$, and C_t takes for the $C_{U(VI)}$ while photocatalysis processing**.**

1.3 The sorption data fitting by isotherm models

Adsorption kinetics were used to analyze the adsorption rate and elucidate the potential rate-controlling mechanism of the adsorption process. To design the appropriate adsorption systems, two well-known kinetics models, pseudo-first-order and pseudo-second-order rate equations are analyzed. The pseudo-first-order and pseudo-second-order equations can be expressed as follows：

$$\ln\left(q_e - q_t\right) = \ln q_e - k_1 t \quad (2)$$

$$\frac{t}{q_t} = \frac{1}{k_2 q_e^2} + \frac{t}{q_e} \quad (3)$$

where t is the contact time (h), q_t and q_e are the amounts of UO_2^{2+} absorbed at time t and at equilibrium (mg/g), respectively, and k_1 (1/h) and k_2 (g/mg h) are the rate constant.

The distribution coefficient K_d was calculated using the following equation:

$$K_d = \frac{(C_0 - C_e)}{C_0} \times \frac{V}{m} \quad (4)$$

Where C_0 and C_e represent the concentration of UO_2^{2+} in the aqueous solution before and after sorption equilibrium, respectively. V and m represent the volume of the aqueous solution and the weight of the dry sorbent, respectively.

1.4 Characterization

Scanning electron microscopy (SEM; Ultra55, Carl Zeiss NTS GmbH, Germany) was used to investigate the surface morphology of Ni-BC@PO_4 composites. Transmission electron microscopy (TEM), high-resolution transmission electron microscopy (HRTEM), and electron diffraction imaging were performed using a field-emission high-resolution transmission electron microscope (FEI Tecnai G2 F20, FEI, USA) at an accelerating voltage of 200 kV. Aberration-corrected electron microscopy was employed for (FEI Theims Z，Titan Cubed Themis G2300，JEM-ARM200F). X-ray diffraction (XRD) patterns of the samples were obtained from 5° to 80° using an X'Pert PRO (PANalytical, The Netherlands) X-ray diffractometer, with Cu Kα (λ=0.15406 nm) radiation, a voltage of 60 kV, a current of 50 mA, and a scan rate of 2°/min. Chemical composition and oxidation state analysis were conducted using a Kratos Axis Ultra photoelectron spectrometer (Thermo escalab 250Xi, Thermo Fisher, USA) with monochromatic Al Kα radiation. Hydroxyl radicals (•OH) and superoxide radicals ($\cdot O_2^-$) were determined by

electron spin resonance (ESR) spectroscopy using a Bruker A300 instrument. X-ray absorption near-edge structure (XANES) measurements were recorded at the beamline BL10B at the National Synchrotron Radiation Laboratory (NSRL) in Hefei, China. Fourier transform infrared spectroscopy (FT-IR) measurements were performed using a Nexus 670 Thermo Nicolet Fourier transform infrared spectrometer in pressed KBr pellets. All electrochemical experiments were conducted at room temperature using a Chi660e electrochemical workstation. Water contact angle measurements were performed with (German Klux K100).

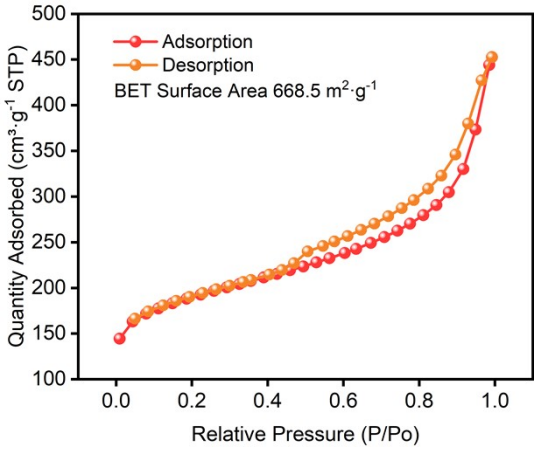

Figure S1. The isothermal adsorption-desorption curve of Ni-BC@PO_4 under nitrogen gas.

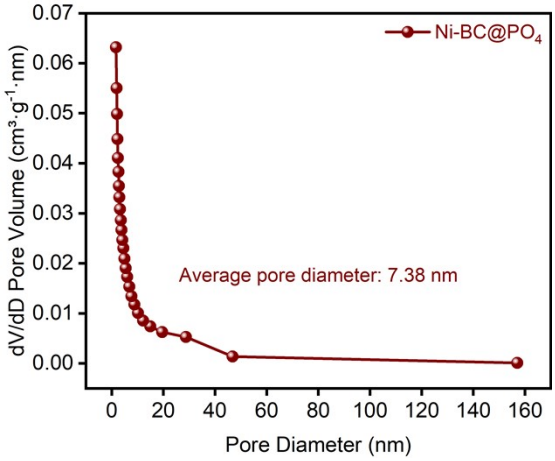

85

86 **Figure S2.** The pore size distribution curve of Ni-BC@PO_4.

87

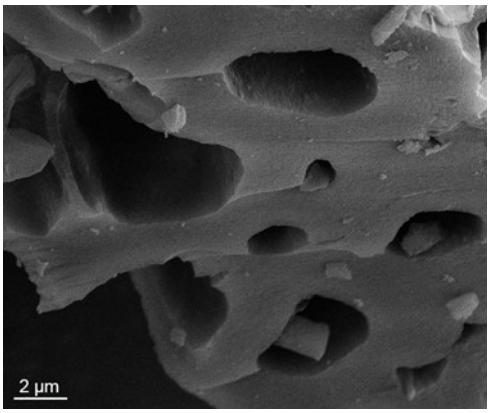

Figure S3. SEM images of BC.

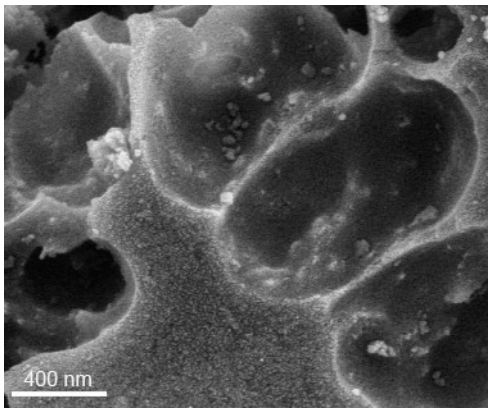

Figure S4. SEM images of Ni-BC@PO_4.

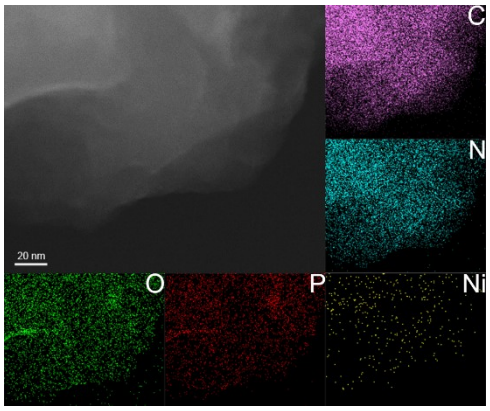

Figure S5. TEM and EDS mapping images of Ni-BC@PO_4 at 20nm.

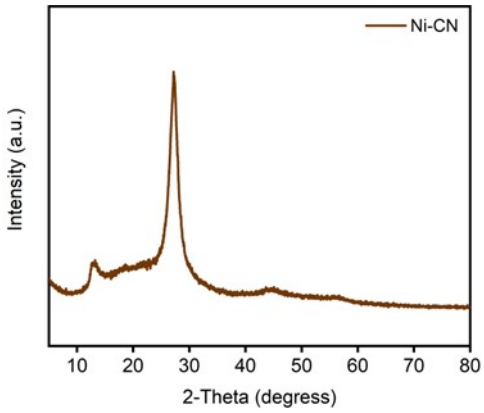

Figure S6. XRD spectrum of Ni-CN.

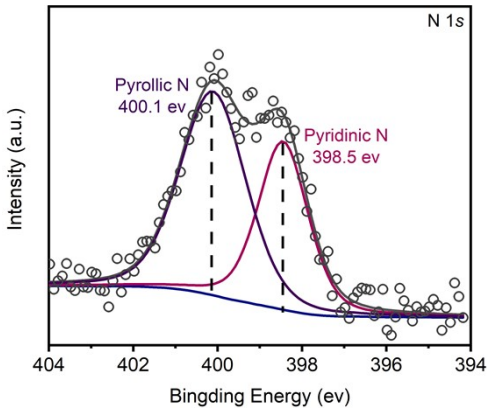

100

101 **Figure S7.** N 1*s* XPS spectra of BC.

102

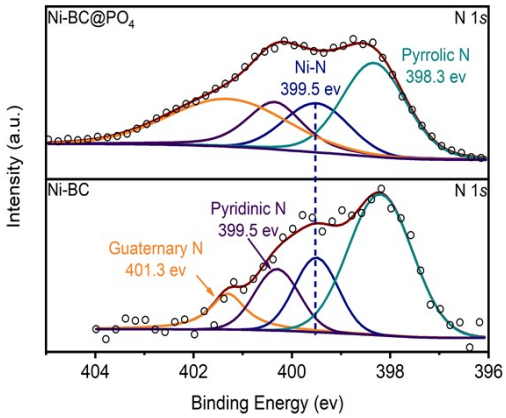

103

104 **Figure S8.** N 1*s* XPS spectra of Ni-BC and Ni-BC@PO_4.

105

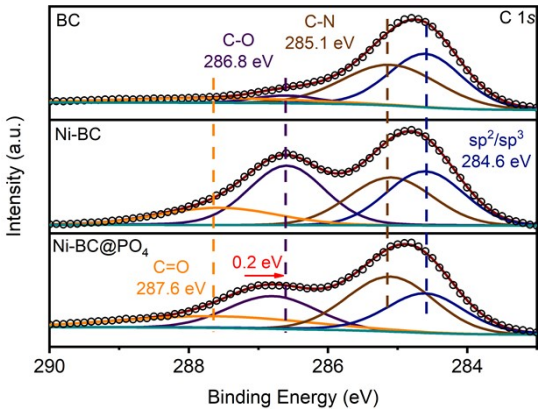

Figure S9. C 1*s* XPS spectra of BC, Ni-BC, and Ni-BC@PO_4.

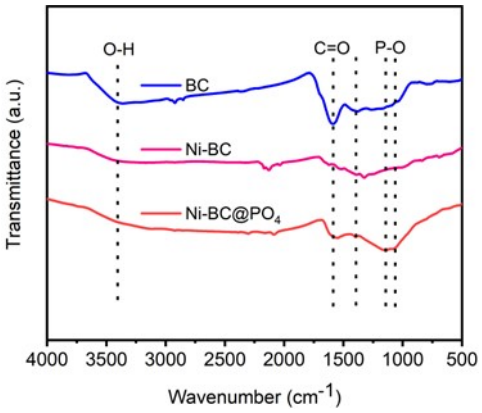

109

110 **Figure S10.** FT-IR spectra of BC, Ni-BC and Ni-BC@PO_4.

111

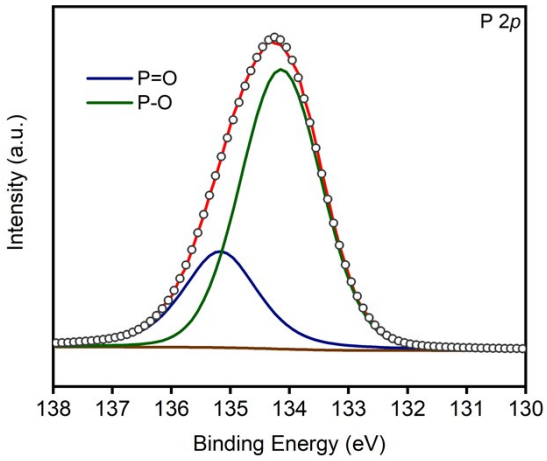

112

113 **Figure S11.** P 2*p* XPS spectra of Ni-BC@PO_4.

114

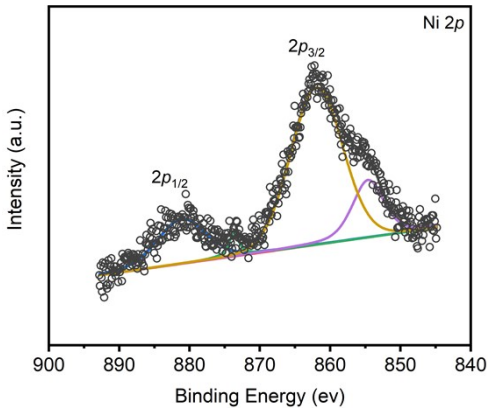

115

116 **Figure S12.** Ni 2*p* XPS spectra of Ni-BC@PO_4.

117

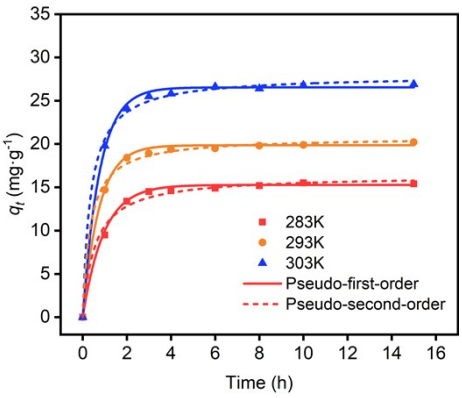

Figure. S13. The adsorption kinetics of uranium by Ni-BC@PO_4 at different temperatures. ($C_{U(VI)}$ = 8 mg/L, m/V = 0.1, T = 283 K, 293K, and 303K, pH = 6.)

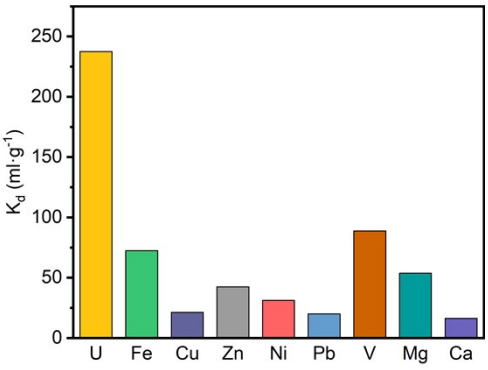

Figure S14. The selectivity of Ni-BC@PO_4 towards uranium in the presence of multiple coexisting ions. ($C_{U(VI)}$ = 8 mg/L, interfering ion concentrations aligned with uranium concentration, m/V = 0.1, T = 293K, pH = 6.)

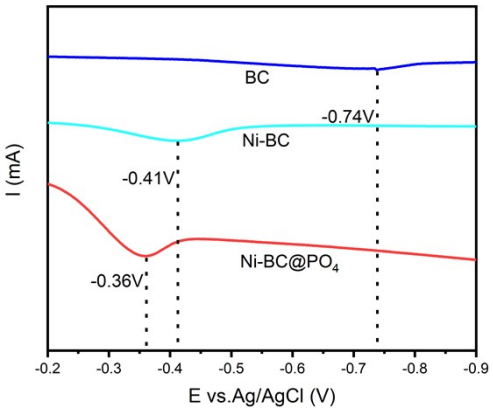

127

128 **Figure S15.** LSV spectra of BC, Ni-BC and Ni-BC@PO_4.

129

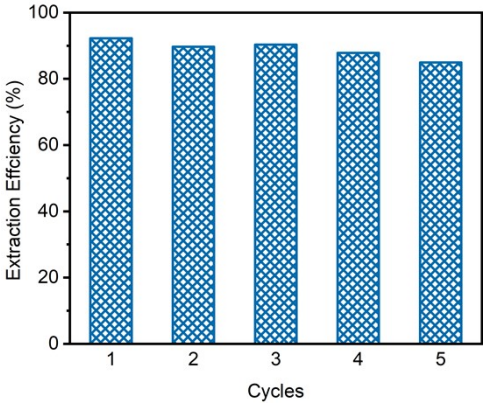

Figure S16. Electrochemical uranium extraction performance of Ni-BC@PO_4 with respect to the number of cycles.

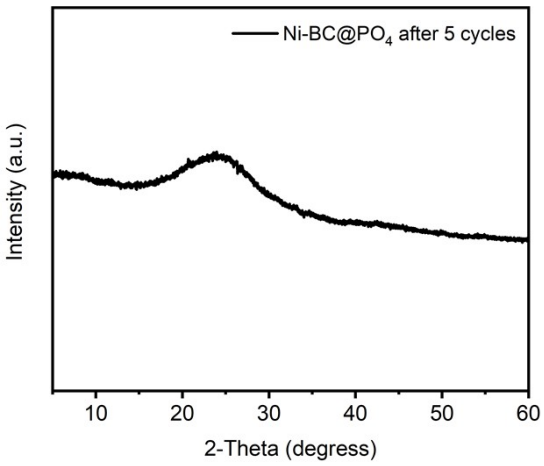

Figure S17. XRD spectrum of Ni-BC@PO_4 after 5 cycles.

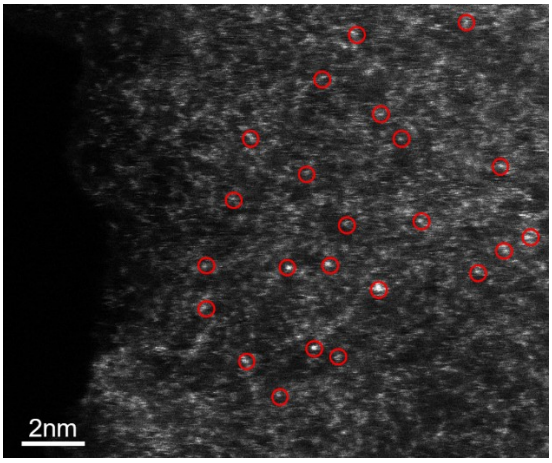

Figure S18. AC-TEM of Ni-BC@PO_4 after 5 cycles.

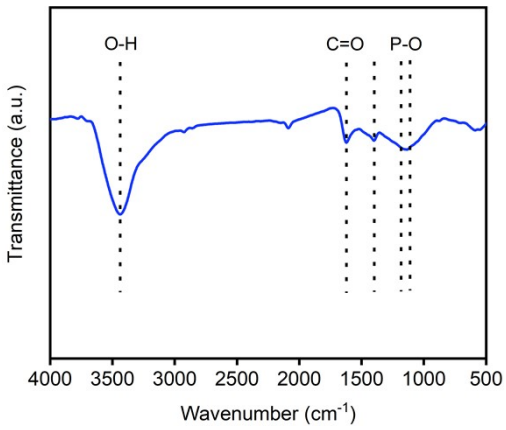

140

141 **Figure S19.** FT-IR spectrum of Ni-BC@PO_4 after 5 cycles.

142

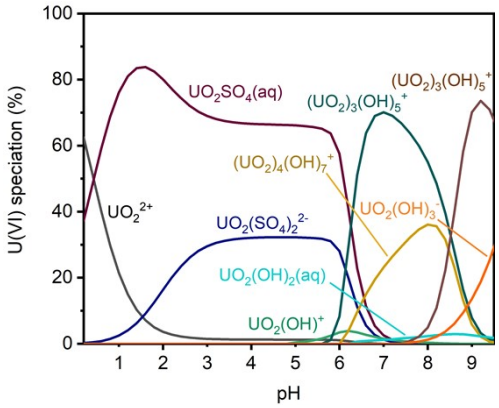

Figure S20. Simulating the response of uranium species in seawater to pH changes.

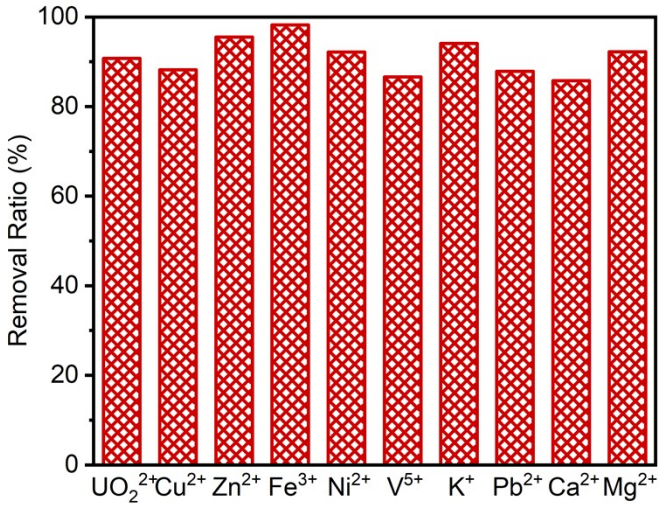

147

148 **Figure S21.** Electroextraction performance of Ni-BC@PO_4 for U(VI) in uranium solutions with
149 competitive cations and its removal effect on U(VI). ($C_{U(VI)}$ = 8 mg/L, $C_{K(I)}$ = 400mg/L, the
150 concentration of other interfering ions is consistent with that of uranium, m/V = 0.1, T = 293K,
151 pH = 5.5).

152

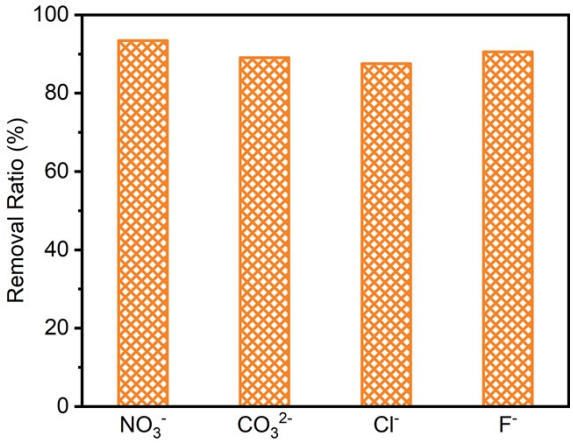

Figure S22. Electroextraction performance of Ni-BC@PO4 for U(VI) in uranium solutions with competitive anions and its removal effect on U(VI). (The concentration of interfering ions is 0.1 M 0.1 M, m/V = 0.1, T = 293K).

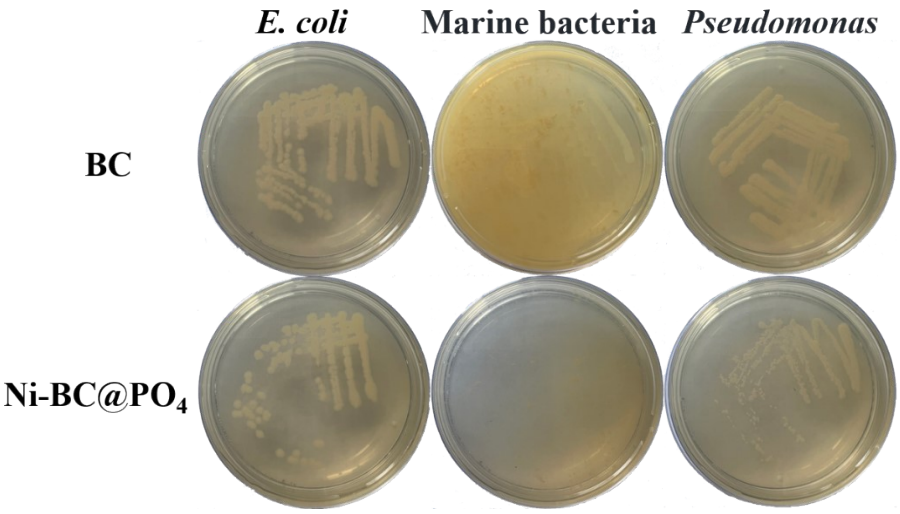

Figure. S23. Antibacterial evaluation of BC and Ni-BC@PO_4.

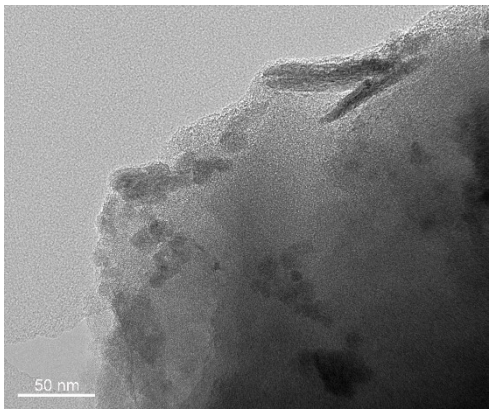

Figure S24. TEM images of Ni-BC@PO_4-U.

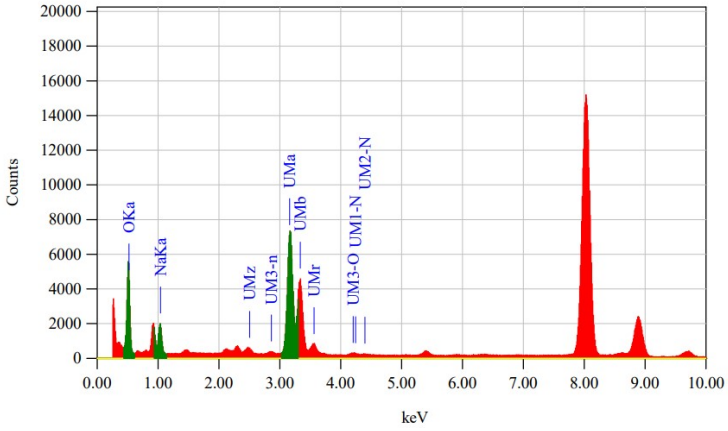

Figure S25. EDX spectra of Ni-BC@PO_4-U.

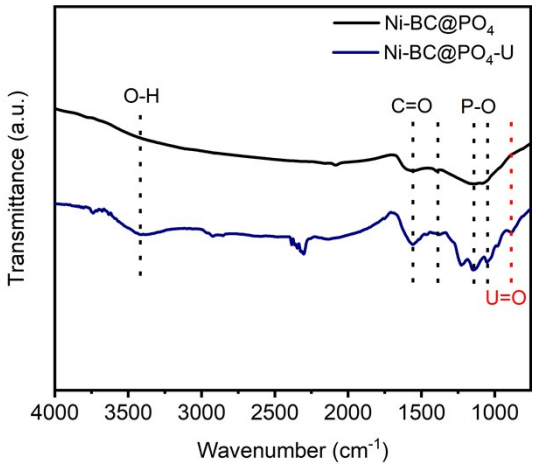

168

169 **Figure S26.** FT-IR spectra of Ni-BC@PO_4-U.

170

Table S1. Comparison of EUE property of the Ni-BC@PO_4 with recently reported catalysts.

Catalyst	Time (d)	enrichment capacity	Ref.
Ni-BC@PO_4	0.5	2.86 $mg \cdot g^{-1} \cdot d^{-1}$	This work
Zn^{2+}-PAO	28	0.33 $mg \cdot g^{-1} \cdot d^{-1}$	[S11]
B-ZnO/ZnInS4	18	0.22 $mg \cdot g^{-1} \cdot d^{-1}$	[S7]
Fe-N-C	1	1.2 $mg \cdot g^{-1} \cdot d^{-1}$	[S15]
NDA-TN-AO	27	0.23 $mg \cdot g^{-1} \cdot d^{-1}$	[S12]
PAO-Co	42	0.23 $mg \cdot g^{-1} \cdot d^{-1}$	[S23]
DNA-UEH	6	1.01 $mg \cdot g^{-1} \cdot d^{-1}$	[S6]

Table S2. Materials and cost required for preparing 1g of Ni-BC@PO_4

Raw Material	Price per unit	Quantity	Total price
R. japonicum L	free	3.743g	free
$C_2H_4N_2$	\$0.173/g	1.387g	\$0.239
$NiCl_2 \cdot 6H_2O$	\$0.074/g	1.387g	\$0.103
70% phytic acid	\$0.069/mL	11.1mL	\$0.766
Total	/	/	\$1.108

The maximum enrichment capacity of Ni-BC@PO_4 for uranium is 927.6mg/g. Taking into account performance losses during the cycling process, the enrichment capacity for each of the five cycles is considered to be 90% of the maximum enrichment capacity. Therefore, the material required for extracting 1kg of uranium is 1.197kg. The cost of uranium extraction per unit mass is \$264/kg.

Excluding material costs, the main source of energy consumption is the electrochemical uranium extraction process. The electrochemical uranium extraction is carried out at a constant voltage of -1.8V, and therefore, integrating the i-t graph yields an approximate energy consumption of 0.977 kW·h per uranium extraction cycle. With five cycles in total, the energy requirement amounts to 4.885 kW·h, resulting in an electricity cost of \$0.396.